The effect of axial compression and distraction on cervical facet mechanics during anterior shear, flexion, axial rotation, and lateral bending motions

Ryan D. Quarrington, John J. Costi, Brian J.C. Freeman, Claire F. Jones

PII: S0021-9290(18)30884-4
DOI: https://doi.org/10.1016/j.jbiomech.2018.11.047
Reference: BM 8956

To appear in: *Journal of Biomechanics*

Received Date: 25 April 2018
Revised Date: 21 November 2018
Accepted Date: 27 November 2018

Please cite this article as: R.D. Quarrington, J.J. Costi, B.J.C. Freeman, C.F. Jones, The effect of axial compression and distraction on cervical facet mechanics during anterior shear, flexion, axial rotation, and lateral bending motions, *Journal of Biomechanics* (2018), doi: https://doi.org/10.1016/j.jbiomech.2018.11.047

TITLE: The effect of axial compression and distraction on cervical facet mechanics during anterior shear, flexion, axial rotation, and lateral bending motions

KEY WORDS: Cervical spine; Biomechanics; Facet joint; Distraction; Compression

WORD COUNT: 3709 words

MANUSCRIPT TYPE: Original Article

AUTHORS:

Ryan D Quarrington, B. Eng (Mechanical and Sports) - Corresponding Author

School of Mechanical Engineering, The University of Adelaide

Centre for Orthopaedic & Trauma Research, Adelaide Medical School, The University of Adelaide

Adelaide Spinal Research Group, Adelaide Medical School, The University of Adelaide

Address: Level 7, Adelaide Health and Medical Sciences Building, North Terrace, Adelaide, SA, 5000

Email: ryan.quarrington@adelaide.edu.au

Phone: +61882223106

John J Costi, PhD

Biomechanics and Implants Research Group, The Medical Device Research Institute, College of Science and Engineering, Flinders University

Address: GPO Box 2100, Adelaide, South Australia 5001, Australia

Email: john.costi@flinders.edu.au

Phone: +61882013323

Brian J C Freeman, MB, BCh, BAO, FRCS (Tr & Orth), FRACS (Ortho), DM

Spinal Injuries Unit, Royal Adelaide Hospital, Adelaide, South Australia

Centre for Orthopaedic & Trauma Research, Adelaide Medical School, The University of Adelaide

Adelaide Spinal Research Group, Adelaide Medical School, The University of Adelaide

Address: Spinal Injuries Unit, Level 5G, Royal Adelaide Hospital, Port Road, Adelaide, SA 5000, Australia

Email: brian.freeman@sa.gov.au

Phone: +61429120991

Claire F Jones, PhD

Centre for Orthopaedic & Trauma Research, Adelaide Medical School, The University of Adelaide

Adelaide Spinal Research Group, Adelaide Medical School, The University of Adelaide

School of Mechanical Engineering, The University of Adelaide.

Address: Level 7, Adelaide Health and Medical Sciences Building, North Terrace, Adelaide, SA, 5000

Email: claire.jones@adelaide.edu.au

Phone: +61883132850

ABSTRACT

The subaxial cervical facets are important load-bearing structures, yet little is known about their mechanical response during physiological or traumatic intervertebral motion. Facet loading likely increases when intervertebral motions are superimposed with axial compression forces, increasing the risk of facet fracture. The aim of this study was to measure the mechanical response of the facets when intervertebral axial compression or distraction is superimposed on constrained, non-destructive shear, bending and rotation motions. Twelve C6/C7 motion segments (70±13 yr, nine male) were subjected to constrained quasi-static anterior shear (1 mm), axial rotation (4°), flexion (10°), and lateral bending (5°) motions. Each motion was superimposed with three axial conditions: 1) 50 N compression; 2) 300 N compression (simulating neck muscle contraction); and, 3) 2.5 mm distraction. Angular deflections, and principal and shear surface strains, of the bilateral C6 inferior facets were calculated from motion-capture data and rosette strain gauges, respectively. Linear mixed-effects models (α=0.05) assessed the effect of axial condition. Minimum principal and maximum shear strains were largest in the compressed condition for all motions except for maximum principal strains during axial rotation. For right axial rotation, maximum principal strains were larger for the contralateral facets, and minimum principal strains were larger for the left facets, regardless of axial condition. Sagittal deflections were largest in the compressed conditions during anterior shear and lateral bending motions, when adjusted for facet side.

KEY WORDS: Cervical spine; Biomechanics; Facet joint; Distraction; Compression

INTRODUCTION

The primary function of the cervical spine is to support and orientate the head. This function is facilitated by the anatomy of the vertebral body and facet joints, and the surrounding ligaments and musculature. In the subaxial cervical spine, intervertebral kinematics are predominantly dictated by the facet joints, where contact between articulating facets prevents excessive axial rotation, lateral bending, and anterior shear (Bogduk and Mercer, 2000). The geometry of the cervical facets is responsible for coupled motions in axial rotation and lateral bending, and is related to the instantaneous axes of rotation observed in the subaxial cervical spine (Bogduk and Mercer, 2000; Nowitzke et al., 1994). In addition, the facet joints bear up to 64% of the axial load in the neutral cervical spine (Pal and Sherk, 1988) and this proportion increases during physiological motion (Panzer and Cronin, 2009). Facet fracture is frequently associated with other cervical injuries (Dvorak et al., 2007), suggesting that high loads are transferred through these joints during trauma.

Despite their important role in cervical kinematics and load-bearing, little is known about the mechanical response of the cervical facets during physiological or non-physiological intervertebral motion. Facet surface strains have been measured during non-traumatic anterior shear motion of cervical functional spinal units (FSUs) (Cripton, 1999), but have not been reported for other intervertebral motions. In a recent study, surface strain, deflection, stiffness and failure load of the subaxial inferior facets were quantified during uni-axial loading that simulated *physiologic* intervertebral flexion and anterior shear motions (Quarrington et al., 2018); however, point loads were applied to the articular facet surfaces, which may not accurately represent *in-vivo* conditions. The response of the cervical facets to *axial rotation* and *lateral bending* has not been investigated. Such measures are required for the validation

of computational models of physiological cervical spine motion and to improve fundamental understanding of cervical spine biomechanics.

Facet fractures are associated with up to 70% of cervical facet dislocations (CFD) (Anissipour et al., 2017; Dvorak et al., 2007); however, facet fracture has not been reported during the experimental production of CFD in cadavers. This may be due to a lack of muscle forces, restricting intervertebral separation (Foster et al., 2012). Such muscle forces may impose an additional intervertebral compressive load during injury that restricts traumatic flexion and intervertebral separation, causing increased loading of the facets. In contrast, superimposed intervertebral *distraction* during traumatic cervical motion, such as that observed during inertially-produced CFD (Ivancic et al., 2008; Panjabi et al., 2007), may reduce loading of the facets, thereby reducing the likelihood of concomitant facet fracture. The effect of axial compression, versus distraction, on the loading of the facets during intervertebral motion has not previously been reported.

The aim of this study was to quantify the mechanical response of the C6 inferior facets in C6/C7 FSUs during constrained, non-destructive, quasi-static anterior shear, axial rotation, lateral bending, and flexion motions (within physiological limits), and to determine the effect of intervertebral axial distraction and compression when imposed on these motions. We hypothesize that axial compression will increase loading of the facets (as measured by deflection and surface strain) when superimposed on shear, bending and rotation motions.

METHODS

Specimen preparation

Cervical motion segments (C5-T1 or C6/C7) were dissected from twelve fresh-frozen human cadavers (mean donor age 70±13 years, range 46-88; nine male) and non-osteoligamentous tissue was removed. High-resolution computed tomography (CT) scans (SOMATOM Force, Siemens, Erlangen, Germany; 0.23×0.23×0.4 mm voxel size) were obtained and each specimen was screened for excessive degeneration, injury or disease by a senior spinal surgeon. Mean volumetric bone mineral density (vBMD) of the anterior third of the C6 and C7 vertebral bodies was determined using a calibration phantom (Mindways Software Inc., Texas, USA) and image analysis software (FIJI 1.51p, ImageJ, Maryland, USA) (Schindelin et al., 2012). Vertebral endplate depths, and facet heights and sagittal angles, were also measured using FIJI.

For Tests #1-5, the distal levels of C5-T1 motion segments were augmented with screws/wire to assist with fixation in blocks of polymethylmethacrylate (PMMA; Vertex Dental, Utrecht, Netherlands). For Tests #6-12, the exposed endplates and posterior elements of C6/C7 FSUs were similarly augmented, and the distal third of each vertebra were embedded. All C6/C7 joints and disco-ligamentous tissues were maintained.

A custom alignment jig ensured that specimens were consistently aligned during embedding, with 22 mm of separation between the molds and 8 mm between the inferior mold and the center of the C6/C7 intervertebral disc (Figure 1); this ensured that the center-of-rotation (CoR) of the flexion-extension axis of the test machine coincided with the CoR of C6/C7 flexion (Penning, 1960), and that the shear force and moment distribution across the intervertebral joints was consistent for all specimens.

Mechanical loading

Each specimen was fixed to a six-axis materials testing machine (8802, Instron, High Wycombe, UK) in an inverted posture (Figure 1). The mold containing the inferior vertebra was fixed to the upper flexion-extension actuator, and the superior vertebra was secured to a six-axis load cell (MC3A-6-1000 ±4.4 kN, AMTI, Massachusetts, USA) mounted on a motorized X-Y table on the base of the testing machine.

Each specimen underwent constrained shear and bending motions under three axial loading conditions. The 'neutral' condition replicated physiological *in vivo* loading (due to head-weight only) by applying a 50 N axial compression force (Bell et al., 2016; DiAngelo and Foley, 2004). For the 'compressed' condition, a 300 N compression force was applied to simulate the loading experienced due to neck muscle bracing; muscle activation can produce intervertebral axial compression forces between 100-1400 N (Bell et al., 2016; Chancey et al., 2003; Cripton et al., 2001; Hattori, 1981; Newell et al., 2014; Pospiech et al., 1999). The 300 N load did not produce off-axis loads exceeding the design limits of the test machine. Finally, 2.5 mm of axial distraction (relative to the neutral position) mimicked the largest non-destructive intervertebral separation previously reported for cervical motion segments (Shea et al., 1991). The location of these axial forces/displacements remained constant throughout each motion.

Prior to testing, the axial actuator *position* corresponding to 10 N of axial load and 0 N or Nm off-axis loads ('unloaded position'), and for each axial condition (50 N, 300 N, 2.5 mm distraction), were recorded. The vertical actuator position of each axial condition was maintained while the specimen underwent three repetitions of anterior shear (1 mm, 0.1

mm/s), flexion (10°, 1 °/s), right axial rotation (4°, 1 °/s) and left lateral bending (5°, 1 °/s); the displacement/rotation limits were based on *in-vivo* ranges of motion (Lin et al., 2014; Penning and Wilmink, 1987; Salem et al., 2013; Wu et al., 2007). The displacement rates were selected to optimize motion-capture frame rate. The order of application of the axial conditions and the motions were block randomized for each specimen. A two-second "hold" was applied at the peak of each rotation/displacement and between each motion. Specimen hydration was maintained using saline-soaked gauze and saline spray.

Instrumentation and data collection

The bases of the bilateral inferior facets of C6 were instrumented with tri-axial strain gauges (FRA-1-23-1L, TML, Tokyo, Japan). The infero-lateral corners of the C6 inferior facets were exposed by resecting a small section of the facet capsule (<3×3 mm) and light-weight motion capture marker-carriers were attached to the bone surface using cyanoacrylate adhesive (Loctite 401, Henkel, Düsseldorf, Germany) (Figure 2). Marker-carriers were attached to the C6 and C7 vertebral bodies with K-wires, and to the superior and inferior molds (Figure 1). Anatomical landmarks on the vertebral bodies and the C6 inferior facets were digitized (Figure S1). Loads, actuator positions, and strain gauge data were collected at 600 Hz using a data acquisition system (PXIe-1073, BNC-2120 & PXIe-4331 (x2), National Instruments, USA). Motion capture data were acquired at 200 Hz (Optotrak Certus, Northern Digital Inc., Ontario, Canada; system bias < 0.09°, precision = 0.006°).

Data processing

Data were processed using custom MATLAB code (R2015a, Mathworks, Massachusetts, USA). Load, position, and strain data were filtered using a second-order, two-way

Butterworth low-pass filter with a cut-off frequency of 100 Hz. Motion capture data were filtered similarly, with a cut-off frequency of 30 Hz.

Peak load (force/moment), maximum and minimum principal strains, maximum shear strains, and angular facet deflections were calculated at the position limit of the last repetition, for each axial condition. Local vertebral body and facet coordinate systems were defined (Figure S1) (Wu et al., 2002). Sagittal, transverse, and coronal angular deflection of the bilateral C6 inferior facets, relative to the C6 vertebral body, were calculated by solving for Euler angles using a *z-y-x* sequence (Robertson, 2004).

Statistics

Statistical analyses were performed using SPSS v24 (IBM, Illinois, USA). For each motion, seven linear mixed-effects models (LMMs) were developed to identify if axial condition was significantly associated with the following outcome measures: 1) peak load; 2) maximum principal strain; 3) minimum principal strain; 4) maximum shear strain; 5) sagittal facet deflection; 6) transverse facet deflection; and, 7) coronal facet deflection. The effect of axial condition was assessed in all models, and this effect was adjusted for facet side (left versus right), donor demographics, specimen bone mineral density, vertebral body size, facet height and angle, order of test condition and imposed axial condition, and the type of specimen (four- versus two-vertebrae). A random effect of facet side, nested within cadaver ID, was included. Shapiro-Wilk and Levene's tests evaluated normality and homogeneity of variance of the dependent variable for each model, and statistically significant outliers were removed and/or data was log-transformed to meet these criteria. Each model was refined using a manual backward step-wise approach until only significant predictors remained (α=0.05).

Bonferroni-adjusted post-hoc comparisons of estimated marginal means (EMMs) were performed for significant categorical predictors.

RESULTS

Demographic information and geometric measurements for the 12 specimens are provided in Table 1. The average load-displacement plots for each axial condition and test direction are illustrated in Figure 3. The neutral and compressed conditions corresponded to mean intervertebral axial compressions (relative to the unloaded position) of 0.13±0.01 and 0.62±0.06 mm, respectively, while 2.5 mm of distraction applied a mean tensile force of 456.66±50.54 N. Off-axis loads are illustrated in Figures S2-S5 in supplementary material. A summary of the final multivariable LMMs is presented in Table 2; the final number of specimens per group, and EMMs and *p*-values from post-hoc comparisons, are provided in Tables S1-S4 in supplementary material.

Axial condition was significantly associated with peak load for the anterior shear and axial rotation motions (Table 2). During these motions, peak loads were largest for the compressed condition, lower for the neutral condition, and lowest for the distracted condition (Figure 4). No significant association was found between axial condition and peak load for flexion and lateral bending.

Intervertebral distraction and compression did not significantly affect maximum principal facet strains but were associated with a difference in minimum principle strains for all motions except axial rotation, when adjusted for gender (Table 2). Maximum principal strains were significantly greater for the ‘unloaded’ right facet during right axial rotation, while minimum principal strains were largest for the left facet (Figure 5). Maximum shear strains

were greatest during the tests with imposed compression for anterior shear (when adjusted for gender and axial order), axial rotation (when adjusted for age) and lateral bending (Table 2). This difference was observed during flexion for the left facets only (Figure 5).

Sagittal facet deflections differed significantly between the left and right facets for all motions except flexion (Table 2). For anterior shear, the magnitude of negative sagittal deflections (anticlockwise about the z-axis and away from the vertebral body) were significantly larger for the compressed and neutral axial conditions when compared to the distracted state and adjusted for facet side and age (Figure 6). A significant difference in sagittal deflections for the neutral versus distracted conditions was also observed during lateral bending, when adjusted for facet side and loading order. The largest magnitude sagittal facet deflections occurred for the left facets during compressed axial rotation (mean: -1.68±0.23°).

Transverse facet deflections were only appreciable during flexion and axial rotation motions. They were significantly higher when compression and neutral axial loads were imposed on flexion motions, compared to the distracted condition, and were larger for the left facet during right axial rotation (when adjusted for gender). Coronal deflections were not appreciable for any load/motion combination.

DISCUSSION

The facets are important load-bearing structures of the subaxial cervical spine, yet their mechanical response during physiological motion is understudied. During cervical trauma, axial compression or distraction can be imposed on pathological intervertebral motions. This may alter facet mechanics and influence the occurrence of concomitant facet fracture (Foster

et al., 2012). In the present study, axial compressions (50 and 300 N) and distraction (2.5 mm) were superimposed on C6/C7 FSUs during constrained intervertebral motions, and the mechanical response of the C6 bilateral inferior facets was measured. In general, the axial compression conditions caused increased loading of the facets, but this was dependent on test direction.

Peak loads were comparable to those observed at corresponding intervertebral displacement/rotation of subaxial cervical FSUs (King Liu et al., 1982; Moroney et al., 1988; Shea et al., 1991). Cripton *et al*. (1999) observed an increase in overall shear stiffness when a compressive preload of 200 N was imposed on anterior shear motion (111.7±13.6 versus 90.9±10.9 N/mm without axial preload). This is consistent with the current study, as significantly larger peak anterior shear loads were observed at 1 mm displacement for the compressed compared to neutral condition (166.7±17.2 vs 130.0±15.3 N, Figure 4a).

The magnitude of *minimum* principal strains was significantly larger for the compressed and neutral conditions, compared to the distracted state, for all motions except axial rotation. However, *maximum* principal strains were not significantly affected by axial condition, and their magnitudes were generally lower than the minimum principal strains (Figure 5). The increase in strain magnitude with axial compression is likely a result of greater facet contact, indicating that the posterior inferior facet bases experience predominantly compressive stresses during facet articulation.

Maximum principal and shear facet surface strains (for the neutral condition) were larger than those observed at the bilateral facet bases during loading of isolated subaxial cervical facets that simulated non-destructive anterior shear motions (maximum principal: 216±39 vs

124±16 με; maximum shear: 602±121 vs 206±29 με) and flexion rotations (maximum principal: 336±72 vs 70±8 με; maximum shear: 712±144 vs 109±15 με) (Quarrington et al., 2018). Maximum and minimum principal strains during anterior shear translations were also generally larger for the current study compared to those measured at the postero-lateral surface of subaxial cervical *superior* facets during unconstrained anterior shear (Cripton, 1999), despite larger intervertebral shear displacement (mean 2 mm) in the latter study. In the latter, the lack of constraints permitted flexion of up to 2° which may have transferred load from the facets to the intervertebral disc, reducing surface strain on the posterior elements. The difference in facet principal strain measurements demonstrates the importance of constrained versus unconstrained intervertebral motion and may provide insight into how facet fractures are associated with dislocation injuries.

During left lateral bending, minimum principal strains were significantly different between each axial condition, and maximum shear strains were significantly larger for the compressed condition compared to the distraction condition (Figure 5d&f). Despite being an asymmetric motion, no significant difference between facet sides was observed for any strain measurements. In contrast, the principal strain responses of the left and right facets were significantly different during right axial rotation, and the effect of axial condition was not significant (Figure 5a&c). Maximum principal strains were larger for the 'unloaded' right facets, presumably due to the facet capsule restricting joint separation, whilst minimum principal strains were of greater magnitude for the loaded left facets due to bony contact (when adjusting for gender). Adjusting for age, maximum shear strains associated with axial rotation *were* significantly larger for the compressed and neutral conditions, compared to distraction (Figure 5f, Table 2). This result was independent of facet side, demonstrating that

the strains experienced by the 'loaded' facet due to bony contact are comparable to those experienced by the contralateral facet due to the capsule.

Sagittal facet deflections were significantly asymmetric throughout all motions except flexion (Figure 6a-d). The left facet deflected more than the right during anterior shear (when adjusting for age), although this significant difference may be an artefact of performing repeated experiments on a small number of specimens. It was hypothesized that this anomaly may be due to sidedness of facet geometry, but these measurements were not significant covariates in the final LMM (Table 2). The magnitude of the sagittal deflections during combined compression-flexion were comparable to those reported by Quarrington *et al*. (2018) (0.25±0.18° vs 0.17±0.01°); however, the sagittal deflections observed during compression-imposed anterior shear were substantially larger (L&R averaged = 0.44±0.11° vs 0.20±0.02°), probably due to the relatively low load (47 N) applied to the facets in that study. Larger deflections during anterior shear displacement with axial compression are consistent with higher compressive and maximum shear strain magnitudes for these tests, supporting the conclusion that the facets experience greater loading in this condition, compared to the distracted condition.

Right axial rotation produced the largest sagittal deflections; the (loaded) left facets experienced deflections that were greatest during compression, whilst the ipsilateral right facets deflected 0.17±0.30° *towards* the vertebral body when rotation was superimposed with axial distraction. Positive sagittal deflection of the 'unloaded' facet, combined with the large maximum principal strains observed at the facet base, suggests that the capsular ligaments have a substantial impact on cervical facet mechanics during axial rotation.

Axial condition did not significantly affect sagittal or transverse deflections during axial rotation; however, this could be due to the use of Euler angles for calculating deflections. The nature of this method may have caused deflections to be inconsistently distributed between the sagittal and transverse planes for each specimen, due to differences in vertebral geometry. Therefore, a consistent difference in deflections was not associated with axial condition. However, both sagittal and transverse deflections for the compressed and neutral conditions were larger than for the distraction condition, so it is likely that axial compression caused larger *resultant* left facet deflections.

The current study data may help explain why facet fracture has not occurred during the experimental production of CFD in cadavers. Lower cervical bilateral CFDs are associated with intervertebral flexion and anterior shear motions (Hodgson and Thomas, 1980; Ivancic, 2012; Nightingale et al., 2016), whilst loading and anatomical asymmetry likely superimposes intervertebral axial rotation and lateral bending onto the external injury vector, causing unilateral CFD (Allen et al., 1982; Hodgson and Thomas, 1980; Maiman et al., 1983; Roaf, 1960). Facet fractures are associated with up to 70% of CFDs (Anissipour et al., 2017; Dvorak et al., 2007); however, in 170 cervical spine head-first impact tests, only 19 CFDs have been produced and none had associated facet fracture (Foster et al., 2012). This may be due to an absence of neck muscle replication during these experiments (Foster et al., 2012; Hu et al., 2008). In computer simulated head-impact tests, neck muscle activation prior to a potentially injurious event (i.e. bracing for impact) increased peak compressive and shear forces in the lower cervical spine, when compared to no muscle activation (Nightingale et al., 2016). The current study demonstrates that simulating neck muscle bracing by superimposing an axial compression force =onto the intervertebral motions associated with bilateral and unilateral CFD (particularly anterior shear and axial rotation) generally increased loading of

the facets. This suggests that increasing these load-motion combinations beyond physiological limits, or applying active neck muscle forces during cervical-spine head impact tests, may produce CFD with facet fracture.

The motions applied in this study were fully constrained, with a fixed CoR, and were applied at quasi-static rates. The flexion, lateral bending, and axial rotation motors were aligned with the average physiological CoR of each motion for C6/C7 FSUs (Anderst et al., 2015; Penning, 1960) and this CoR was consistent for each axial condition, but the testing machine used in the current study was unable to alter the axis-of-rotation throughout the motion, as occurs *in-vivo*. In addition, physiological cervical motions are coupled with off-axis translations and rotations (Lin et al., 2014; Wachowski et al., 2009; Wu et al., 2007). However, motion segments do not exhibit physiological kinematics during cervical trauma (Ivancic et al., 2008; Nightingale et al., 1996; Nightingale et al., 2016; Panjabi et al., 2007), and it is important to obtain quantitative information about the mechanical response of cervical FSUs and the facets during constrained intervertebral motions to develop improved injury tolerance levels. When extrapolating these results beyond physiological limits it is important to recognize that the quasi-static rates applied in this study were substantially slower than the ~3 m/s associated with head-impact loading causing cervical injury (McElhaney et al., 1979; Nightingale et al., 1996; Van Toen et al., 2014). The mechanical behavior of biological tissue is rate-dependent and higher rate displacements would likely increase the stiffness of the facets, intervertebral disc, and other surrounding soft-tissue (McElhaney, 1966). However, while this may reduce the measured deflections and surface strains, it is unlikely to alter the relative effect of axial condition on facet response.

While surface strains and facet tip deflections can provide an indication of the mechanical response of the subaxial cervical facets during intervertebral motions, the inability to directly visualize inter-facet engagement is a limitation of this study. Maintaining surrounding soft-tissue was important to capture biofidelic strain and deflection data, but the presence of these structures prevented observation or measurement of the detailed contact mechanics of the subaxial cervical facet joints.

Approximately one-third of the superior and inferior anatomy of C6 and C7, respectively, were embedded in PMMA. Therefore, the boundary conditions for each vertebra are likely not representative of the *in-vivo* environment, and this may have affected the mechanical response of the posterior elements. However, repeated measures analysis was used to determine the effect of axial condition on this response, and great care was taken to ensure that each specimen was prepared in a consistent manner.

This study provides quantitative information about the mechanical response of the C6 inferior facets during constrained shear and bending motions of C6/C7 FSUs under three axial loading conditions. The response was dependent on test direction, but minimum principal and maximum shear strains, and sagittal deflections, were generally largest in the compressed conditions. This information may assist when validating computational models of cervical spinal motion and improves our understanding of cervical facet biomechanics.

ACKNOWLEDGEMENTS

The authors thank the Data, Design and Statistics Service, The University of Adelaide, for their assistance. Funding was provided by AOSpine Australia New Zealand (AOSAUNZ2015-03), the Royal Adelaide Hospital Research Fund, and the Australian

Government's Research Training Program. CF Jones is supported by a National Health and Medical Research Council (Australia) Early Career Fellowship.

CONFLICT OF INTEREST STATEMENT

No competing financial interests exist.

REFERENCES

Allen, B.L., Jr., Ferguson, R.L., Lehmann, T.R., O'Brien, R.P., 1982. A mechanistic classification of closed, indirect fractures and dislocations of the lower cervical spine. Spine (Phila Pa 1976) 7, 1-27.

Anderst, W.J., Donaldson, W.F., 3rd, Lee, J.Y., Kang, J.D., 2015. Three-dimensional intervertebral kinematics in the healthy young adult cervical spine during dynamic functional loading. J Biomech 48, 1286-1293.

Anissipour, A.K., Agel, J., Baron, M., Magnusson, E., Bellabarba, C., Bransford, R.J., 2017. Traumatic Cervical Unilateral and Bilateral Facet Dislocations Treated With Anterior Cervical Discectomy and Fusion Has a Low Failure Rate. Global Spine J 7, 110-115.

Bell, K.M., Yan, Y., Debski, R.E., Sowa, G.A., Kang, J.D., Tashman, S., 2016. Influence of varying compressive loading methods on physiologic motion patterns in the cervical spine. J Biomech 49, 167-172.

Bogduk, N., Mercer, S., 2000. Biomechanics of the cervical spine. I: Normal kinematics. Clin Biomech (Bristol, Avon) 15, 633-648.

Chancey, V.C., Nightingale, R.W., Van Ee, C.A., Knaub, K.E., Myers, B.S., 2003. Improved estimation of human neck tensile tolerance: reducing the range of reported tolerance using

anthropometrically correct muscles and optimized physiologic initial conditions. Stapp Car Crash J 47, 135-153.

Cripton, P.A., 1999. Load-sharing in the human cervical spine. Queen's University, Kingston, Ontario, Canada.

Cripton, P.A., Dumas, G.A., Nolte, L.P., 2001. A minimally disruptive technique for measuring intervertebral disc pressure in vitro: application to the cervical spine. J Biomech 34, 545-549.

Cusick, J.F., Yoganandan, N., 2002. Biomechanics of the cervical spine 4: major injuries. Clinical Biomechanics 17, 1-20.

DiAngelo, D.J., Foley, K.T., 2004. An improved biomechanical testing protocol for evaluating spinal arthroplasty and motion preservation devices in a multilevel human cadaveric cervical model. Neurosurg Focus 17, E4.

Dvorak, M.F., Fisher, C.G., Aarabi, B., Harris, M.B., Hurbert, R.J., Rampersaud, Y.R., Vaccaro, A., Harrop, J.S., Nockels, R.P., Madrazo, I.N., Schwartz, D., Kwon, B.K., Zhao, Y., Fehlings, M.G., 2007. Clinical outcomes of 90 isolated unilateral facet fractures, subluxations, and dislocations treated surgically and nonoperatively. Spine (Phila Pa 1976) 32, 3007-3013.

Foster, B.J., Kerrigan, J.R., Nightingale, R.W., Funk, J.R., Cormier, J.M., Bose, D., Sochor, M.R., Ridella, S.A., Ash, J.H., Crandall, J., Year Analysis of cervical spine injuries and mechanisms for CIREN rollover crashes. In 2012 International IRCOBI Conference on the Biomechanics of Injury. Dublin, Ireland.

Hattori, S., 1981. Cervical intradiscal pressure in movements and traction of the cervical spine. Z Orthop 119, 568-569.

Hodgson, V., Thomas, L., 1980. Mechanisms of cervical spine injury during impact to the protected head. SAE Technical Paper 801300.

Hu, J., Yang, K.H., Chou, C.C., King, A.I., 2008. A numerical investigation of factors affecting cervical spine injuries during rollover crashes. Spine (Phila Pa 1976) 33, 2529-2535.

Huelke, D.F., Nusholtz, G.S., 1986. Cervical spine biomechanics: A review of the literature. Journal of Orthopaedic Research 4, 232-245.

Ivancic, P.C., 2012. Biomechanics of sports-induced axial-compression injuries of the neck. J Athl Train 47, 489-497.

Ivancic, P.C., Pearson, A.M., Tominaga, Y., Simpson, A.K., Yue, J.J., Panjabi, M.M., 2007. Mechanism of cervical spinal cord injury during bilateral facet dislocation. Spine (Phila Pa 1976) 32, 2467-2473.

Ivancic, P.C., Pearson, A.M., Tominaga, Y., Simpson, A.K., Yue, J.J., Panjabi, M.M., 2008. Biomechanics of cervical facet dislocation. Traffic Inj Prev 9, 606-611.

King Liu, Y., W. Krieger, K., Njus, G., Ueno, K., P. Connors, M., 1982. Cervical Spine Stiffness and Geometry of the Young Human Male.

Lin, C.C., Lu, T.W., Wang, T.M., Hsu, C.Y., Hsu, S.J., Shih, T.F., 2014. In vivo three-dimensional intervertebral kinematics of the subaxial cervical spine during seated axial rotation and lateral bending via a fluoroscopy-to-CT registration approach. J Biomech 47, 3310-3317.

Maiman, D.J., Sances, A., Jr., Myklebust, J.B., Larson, S.J., Houterman, C., Chilbert, M., El-Ghatit, A.Z., 1983. Compression injuries of the cervical spine: a biomechanical analysis. Neurosurgery 13, 254-260.

McElhaney, J.H., 1966. Dynamic response of bone and muscle tissue. J Appl Physiol 21, 1231-1236.

Moroney, S.P., Schultz, A.B., Miller, J.A., Andersson, G.B., 1988. Load-displacement properties of lower cervical spine motion segments. J Biomech 21, 769-779.

Newell, R.S., Siegmund, G.P., Blouin, J.S., Street, J., Cripton, P.A., 2014. Cervical vertebral realignment when voluntarily adopting a protective neck posture. Spine (Phila Pa 1976) 39, E885-893.

Nightingale, R.W., Doherty, B.J., Myers, B.S., McElhaney, J.H., Richardson, W.J., 1991. The influence of end condition on human cervical spine injury mechanisms, SAE Technical Paper 912915.

Nightingale, R.W., McElhaney, J.H., Richardson, W.J., Myers, B.S., 1996. Dynamic responses of the head and cervical spine to axial impact loading. J Biomech 29, 307-318.

Nightingale, R.W., Sganga, J., Cutcliffe, H., Bass, C.R., 2016. Impact responses of the cervical spine: A computational study of the effects of muscle activity, torso constraint, and pre-flexion. J Biomech 49, 558-564.

Nowitzke, A., Westaway, M., Bogduk, N., 1994. Cervical zygapophyseal joints: geometrical parameters and relationship to cervical kinematics. Clinical Biomechanics 9, 342-348.

Pal, G.P., Sherk, H.H., 1988. The vertical stability of the cervical spine. Spine (Phila Pa 1976) 13, 447-449.

Panjabi, M.M., Simpson, A.K., Ivancic, P.C., Pearson, A.M., Tominaga, Y., Yue, J.J., 2007. Cervical facet joint kinematics during bilateral facet dislocation. European Spine Journal 16, 1680-1688.

Panzer, M.B., Cronin, D.S., 2009. C4–C5 segment finite element model development, validation, and load-sharing investigation. Journal of Biomechanics 42, 480-490.

Penning, L., 1960. Functioneel röntgenonderzoek bij degeneratieve en traumatische aandoeningen der laag-cervicale bewegingssegmenten.

Penning, L., Wilmink, J.T., 1987. Rotation of the cervical spine. A CT study in normal subjects. Spine (Phila Pa 1976) 12, 732-738.

Pospiech, J., Stolke, D., Wilke, H.J., Claes, L.E., 1999. Intradiscal pressure recordings in the cervical spine. Neurosurgery 44, 379-384; discussion 384-375.

Quarrington, R.D., Costi, J.J., Freeman, B.J.C., Jones, C.F., 2018. Quantitative evaluation of facet deflection, stiffness, strain and failure load during simulated cervical spine trauma. Journal of Biomechanics 72, 116-124.

Roaf, R., 1960. A study of the mechanics of spinal injuries. Journal of Bone and Joint Surgery 42B, 810-823.

Robertson, D.G.E., 2004. Research methods in biomechanics. Human Kinetics, Champaign, IL.

Salem, W., Lenders, C., Mathieu, J., Hermanus, N., Klein, P., 2013. In vivo three-dimensional kinematics of the cervical spine during maximal axial rotation. Man Ther 18, 339-344.

Schindelin, J., Arganda-Carreras, I., Frise, E., Kaynig, V., Longair, M., Pietzsch, T., Preibisch, S., Rueden, C., Saalfeld, S., Schmid, B., Tinevez, J.-Y., White, D.J., Hartenstein, V., Eliceiri, K., Tomancak, P., Cardona, A., 2012. Fiji: an open-source platform for biological-image analysis. Nat Meth 9, 676-682.

Shea, M., Edwards, W.T., White, A.A., Hayes, W.C., 1991. Variations of stiffness and strength along the human cervical spine. J Biomech 24, 95-107.

Wachowski, M.M., Mansour, M., Lee, C., Ackenhausen, A., Spiering, S., Fanghanel, J., Dumont, C., Kubein-Meesenburg, D., Nagerl, H., 2009. How do spinal segments move? J Biomech 42, 2286-2293.

White, A.A., Panjabi, M.M., 1990. Clinical Biomechanics of the Spine. Lippincott.

Wu, G., Siegler, S., Allard, P., Kirtley, C., Leardini, A., Rosenbaum, D., Whittle, M., D'Lima, D.D., Cristofolini, L., Witte, H., Schmid, O., Stokes, I., 2002. ISB recommendation on definitions of joint coordinate system of various joints for the reporting of human joint motion--part I: ankle, hip, and spine. International Society of Biomechanics. Journal of Biomechanics 35, 543-548.

Wu, S.K., Kuo, L.C., Lan, H.C., Tsai, S.W., Chen, C.L., Su, F.C., 2007. The quantitative measurements of the intervertebral angulation and translation during cervical flexion and extension. Eur Spine J 16, 1435-1444.

Figure 1: Lateral schematic of the embedded specimen attached to the six-axis testing machine in an inverted posture (left) and an oblique photo of the test setup (right). The position of the superior mold was held constant and axial rotation, flexion, and lateral bending motions were individually applied to the inferior mold by their respective rotary motors. Anterior shear motion was applied to the superior mold by the motorized X-Y table. Each motion was combined with either neutral, compressed, or distracted intervertebral separation, which was applied by the axial actuator. Six-axis forces and moments were recorded by the load-cell to which the superior mold was attached. VB = vertebral body, MC = marker carrier.

Figure 2: Prior to embedding the inferior anatomy and screw/wire constructs, Optotrak marker-carriers were fixed to the C6 bilateral inferior facet tips (left) and the C6 inferior facet bases were instrumented with tri-axial rosette strain gauges immediately superior to the C6/C7 facet capsules (right).

Figure 3: Average load-displacement/rotation plots for the loading region of each motion in each axial condition. The shaded regions indicate ±1 standard error.

Figure 4: Mean (±1 S.E.) measured peak: a) anterior shear load; and, b) bending moments for the compressed, neutral, and distracted axial conditions. Outliers that were omitted from statistical analysis are not displayed. Significant differences between axial conditions for each motion, as determined by Bonferroni-adjusted post-hoc analysis of the final multivariable linear mixed-effects models (α=0.05), are indicated.

Figure 5: Mean (±1 S.E.) measured: a) & b) maximum principal strains; c) & d) minimum principal strains; and, e) & f) maximum shear strains for the compressed, neutral, and distracted axial conditions. Outliers that were omitted from statistical analysis are not displayed. Left and right facet measurements are grouped for those outcomes with no significant difference between sides. Significant differences between axial conditions for each motion, as determined by Bonferroni-adjusted post-hoc analysis of the final multivariable linear mixed-effects models (α=0.05), are indicated.

Figure 6: Mean (±1 S.E.) measured: a) – d) sagittal; e) & f) transverse; and, g) coronal facet deflections for the compressed, neutral, and distracted axial conditions, for each motion. Negative angles indicate left transverse and coronal deflections, and sagittal deflections away from the vertebral body. Outliers that were omitted from statistical analysis are not displayed. Left and right facet measurements are grouped for those outcomes with no significant difference between sides. Significant differences between axial conditions for each motion, as determined by Bonferroni-adjusted post-hoc analysis of the final multivariable linear mixed-effects models (α=0.05), are indicated.

Figure S1: Schematics of the inferior (left) and right lateral (right) views of a C6 vertebra and C6/C7 FSU, respectively. The red circles indicate the anatomical landmarks that were digitized. The local coordinate systems are illustrated, with x-axes in red, z-axes in blue, and y-axes in green. The origin of the vertebral body was defined as the sagittal midpoint of the anterior edge of the inferior vertebral endplate. The origin of the facets were defined as the geometric center of the articular surfaces. X indicates an axis directed into the page, while O indicates an axis directed out of the page. VB = vertebral body, RF = right facet, LF = left facet.

Figure S2: Average off-axis load-displacement plots for the loading region of anterior shear motion imposed with each axial condition. The shaded regions indicate ±1 standard error.

Figure S3: Average off-axis load-displacement plots for the loading region of axial rotation motion imposed with each axial condition. The shaded regions indicate ±1 standard error.

Figure S4: Average off-axis load-displacement plots for the loading region of flexion motion imposed with each axial condition. The shaded regions indicate ±1 standard error.

Figure S5: Average off-axis load-displacement plots for the loading region of lateral bending motion imposed with each axial condition. The shaded regions indicate ±1 standard error.

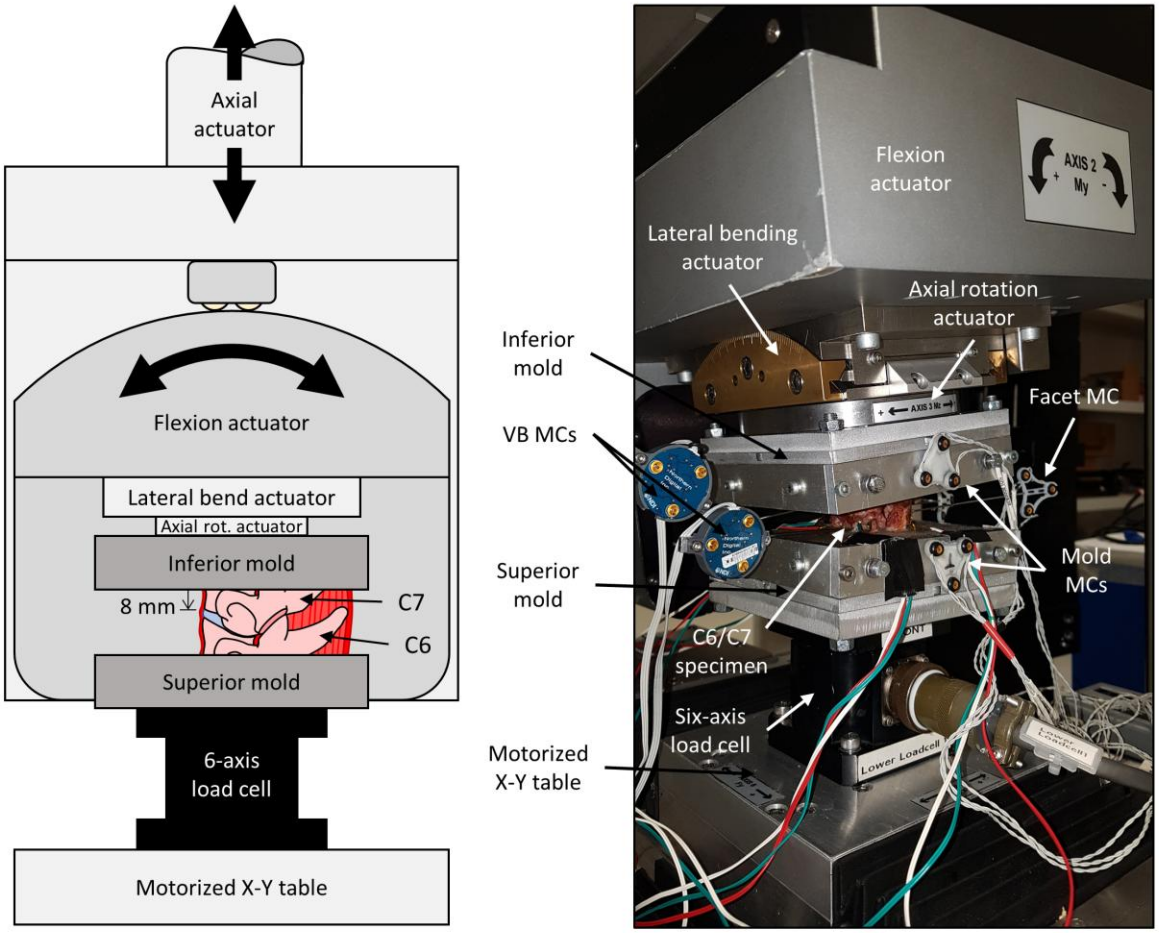

Figure 01 – Suggest double column

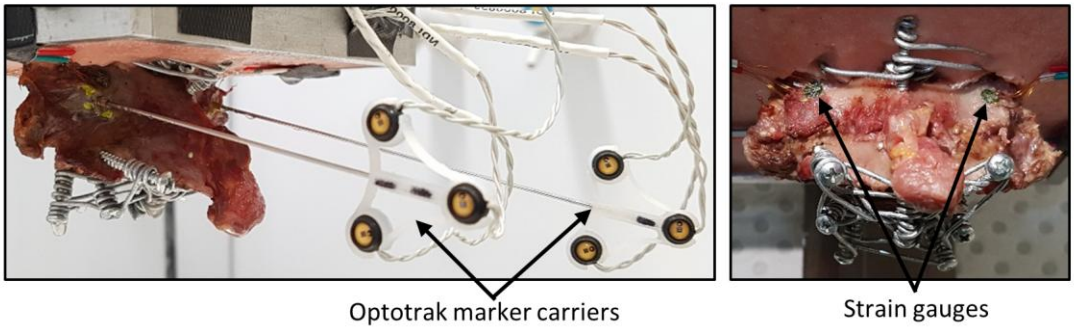

Figure 02 – Suggest 1.5 column

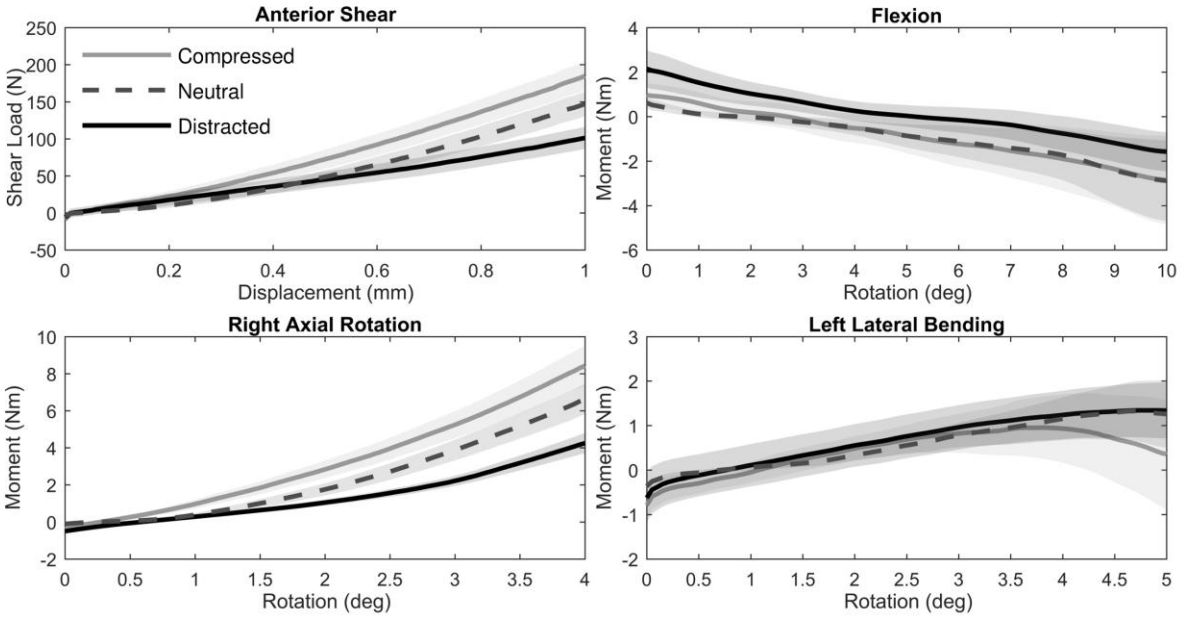

Figure 03 – Suggest double column

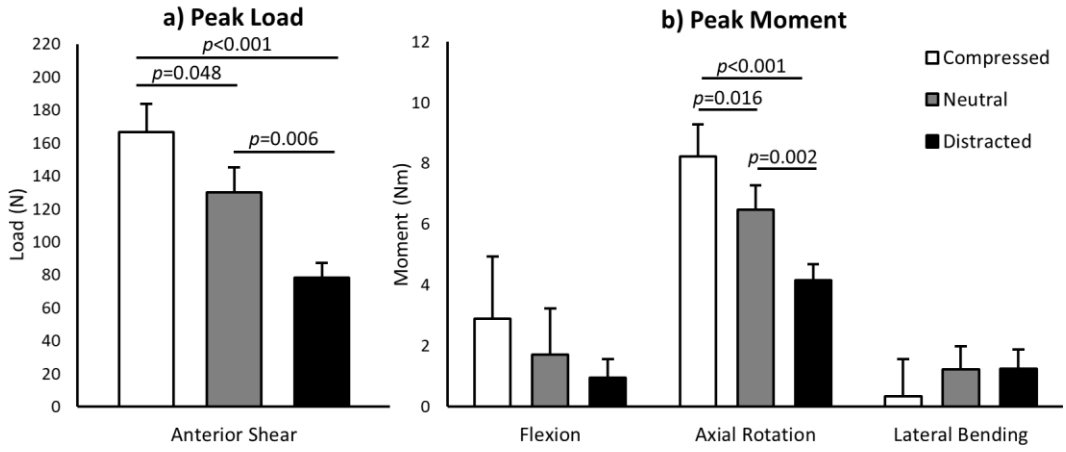

Figure 04 – Suggest 1.5 column

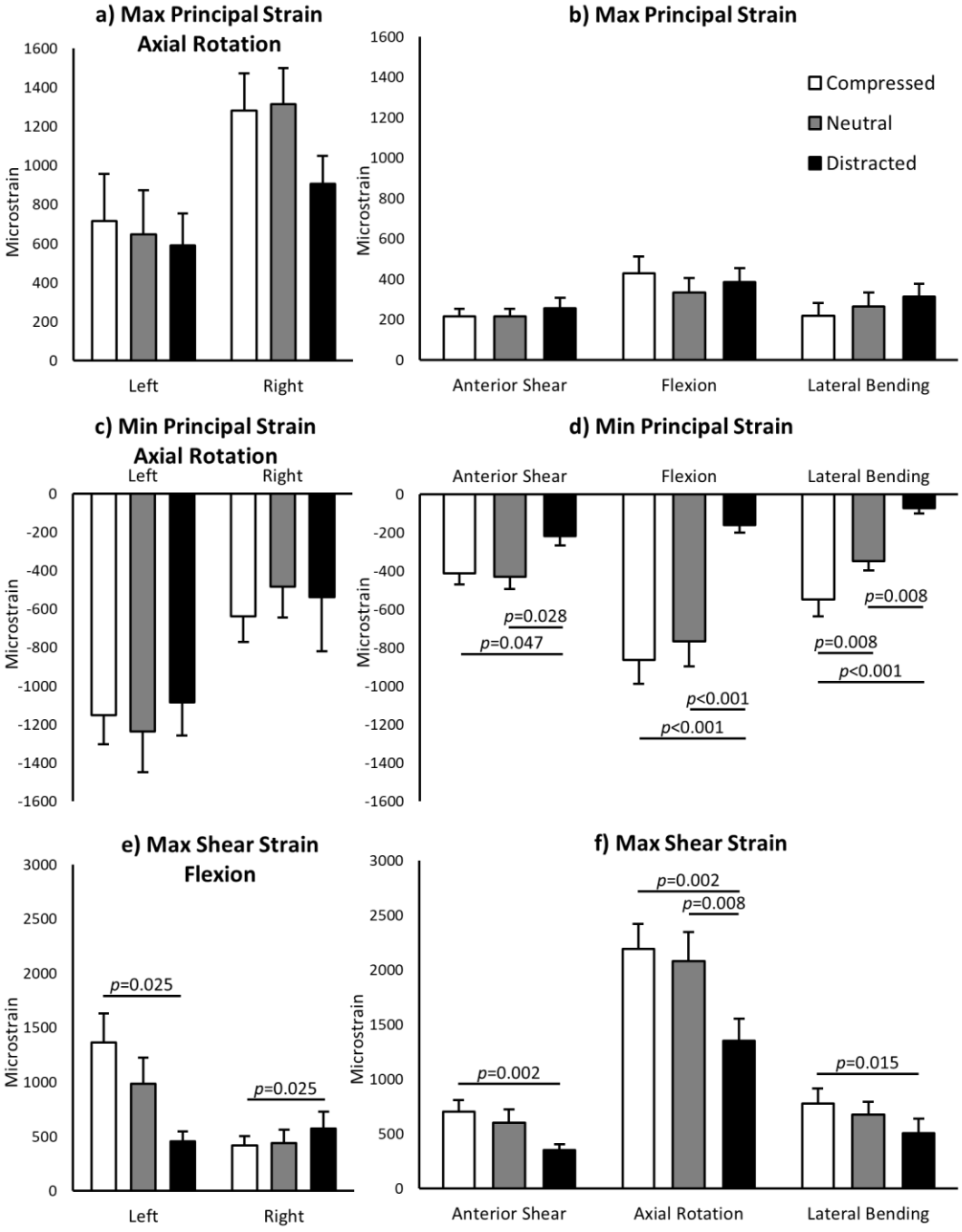

Figure 05 – Suggest 1.5 column

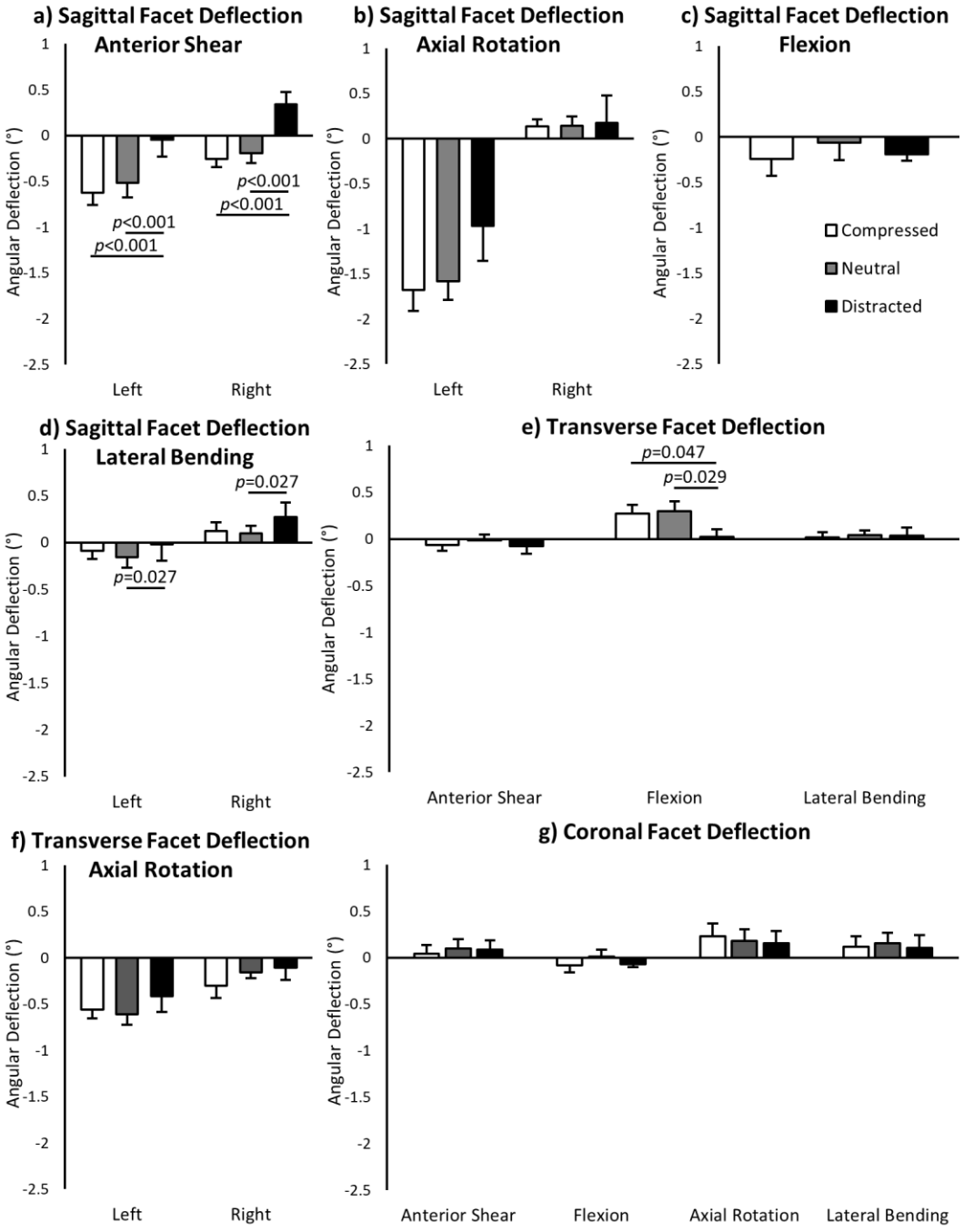

Figure 06 – Suggest 1.5 column

Table 1: Specimen details and geometry. VB = vertebral body. vBMD = volumetric K2HPO4 equivalent bone mineral density.

Test #	Specimen Identifier	Sex	Age	Specimen Type	Left Facet Height (mm)	Right Facet Height (mm)	Left Facet Angle (°)	Right Facet Angle (°)	Mean VB Depth (mm)	Mean vBMD (mg/cm^3)
1	H010	M	71	Four Vertebrae	9.1	9.9	114.1	114.0	16.7	138.8
2	H013	M	58	Four Vertebrae	7.8	5.1	125.6	131.4	15.6	115.0
3	H014	M	58	Four Vertebrae	5.4	9.7	136.0	139.1	17.4	83.6
4	H003	M	46	Four Vertebrae	8.0	7.3	138.3	135.6	15.6	142.9
5	H002	F	62	Four Vertebrae	8.9	11.2	135.4	133.1	16.1	216.7
6	H004	F	75	Two Vertebrae	9.4	11.5	129.1	123.3	16.2	99.0
7	H036	M	58	Two Vertebrae	10.3	8.1	130.2	110.3	17.2	125.5
8	H009	M	85	Two Vertebrae	9.7	8.5	130.4	131.6	19.1	223.5
9	H041	M	82	Two Vertebrae	6.9	8.9	117.5	132.0	15.7	74.1
10	H020	M	76	Two Vertebrae	9.0	11.1	126.3	121.4	16.9	105.2
11	H033	F	88	Two Vertebrae	8.6	5.7	130.9	128.5	16.6	117.1
12	H043	M	81	Two Vertebrae	7.1	7.0	130.5	128.3	17.5	164.4

Table 2: Summary of the final multivariable linear mixed-effects models for each motion. Significant p-values (α=0.05) for the axial condition variable are bolded.

Outcome Variable:	Axial Condition p-Value:	Significant Covariates:
Anterior Shear		
Peak Load	**<0.001**	
Maximum Principal Strain	0.664	
Minimum Principal Strain	**0.025**	
Maximum Shear Strain	**0.004**	Gender, Axial Condition Order
Sagittal Facet Deflection	**<0.001**	Facet Side, Age
Transverse Facet Deflection	0.366	Gender, vBMD, Age
Coronal Facet Deflection	0.742	
Flexion		
Peak Load	0.298	
Maximum Principal Strain	0.529	Axial Condition Order
Minimum Principal Strain	**<0.001**	
Maximum Shear Strain	**0.039**	Facet Side, vBMD, Axial Condition Order
Sagittal Facet Deflection	0.447	vBMD, Facet Height

Transverse Facet Deflection	**0.026**	
Coronal Facet Deflection	0.168	
Axial Rotation		
Peak Load	**<0.001**	
Maximum Principal Strain	0.074	Facet Side
Minimum Principal Strain	0.776	Facet Side, Gender
Maximum Shear Strain	**0.002**	Age
Sagittal Facet Deflection	0.178	Facet Side
Transverse Facet Deflection	0.388	Facet Side, Gender
Coronal Facet Deflection	0.868	Facet Side
Lateral Bending		
Peak Load	0.604	
Maximum Principal Strain	0.277	
Minimum Principal Strain	**<0.001**	
Maximum Shear Strain	**0.016**	
Sagittal Facet Deflection	**0.034**	Facet Side, Axial Condition Order
Transverse Facet Deflection	0.946	
Coronal Facet Deflection	0.947	